

Structural observation of piezoelectric inhomogeneity in a mixed-orientation $\text{Na}_{0.5}\text{Bi}_{0.5}\text{TiO}_3$ perovskite thin film

D. Carbone, A. I. Pateras, G. Bussone, P. G. Evans, T. W. Cornelius, M. Bousquet, A. Boulle, B. Gautier, and J. R. Duclère

Citation: *Applied Physics Letters* **105**, 242901 (2014); doi: 10.1063/1.4904458

View online: <http://dx.doi.org/10.1063/1.4904458>

View Table of Contents: <http://scitation.aip.org/content/aip/journal/apl/105/24?ver=pdfcov>

Published by the AIP Publishing

Articles you may be interested in

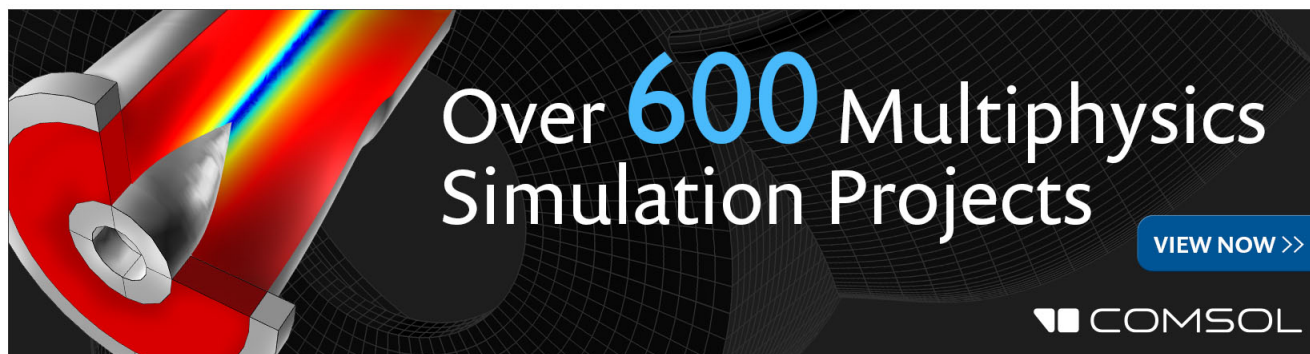
Structural stability and depolarization of manganese-doped $(\text{Bi}_{0.5}\text{Na}_{0.5})_{1-x}\text{Ba}_x\text{TiO}_3$ relaxor ferroelectrics
J. Appl. Phys. **116**, 154101 (2014); 10.1063/1.4898322

Orientation dependence on piezoelectric properties of $\text{Bi}_{0.5}\text{Na}_{0.5}\text{TiO}_3\text{-BaTiO}_3\text{-SrTiO}_3$ epitaxial thin films
Appl. Phys. Lett. **104**, 172903 (2014); 10.1063/1.4874805

Structure and properties of La-modified $\text{Na}_{0.5}\text{Bi}_{0.5}\text{TiO}_3$ at ambient and elevated temperatures
J. Appl. Phys. **112**, 054111 (2012); 10.1063/1.4751357

Electromechanical properties of A-site (LiCe)-modified sodium bismuth titanate ($\text{Na}_{0.5}\text{Bi}_{4.5}\text{Ti}_4\text{O}_{15}$) piezoelectric ceramics at elevated temperature
J. Appl. Phys. **105**, 094110 (2009); 10.1063/1.3117219

Piezoforce microscopy study of lead-free perovskite $\text{Na}_{0.5}\text{Bi}_{0.5}\text{TiO}_3$ thin films
Appl. Phys. Lett. **90**, 152905 (2007); 10.1063/1.2721843

The advertisement features a 3D simulation of a mechanical part with a color gradient from red to blue, indicating stress or temperature distribution. The text 'Over 600 Multiphysics Simulation Projects' is prominently displayed in white and blue. A blue button with white text says 'VIEW NOW >>'. The COMSOL logo is in the bottom right corner.

Over 600 Multiphysics Simulation Projects

VIEW NOW >>

COMSOL

Structural observation of piezoelectric inhomogeneity in a mixed-orientation $\text{Na}_{0.5}\text{Bi}_{0.5}\text{TiO}_3$ perovskite thin film

D. Carbone,^{1,a)} A. I. Pateras,^{1,2,b)} G. Bussone,¹ P. G. Evans,^{3,c)} T. W. Cornelius,^{1,d)} M. Bousquet,^{4,e)} A. Boule,⁴ B. Gautier,⁵ and J. R. Duclère^{4,f)}

¹ID01/ESRF, BP 220, F-38043 Grenoble, France

²Department of Physics, National Technical University of Athens, Zografou Campus, GR-15780 Athens, Greece

³Materials Science and Engineering, University of Wisconsin-Madison, Madison, Wisconsin 53706, USA

⁴SPCTS CNRS UMR 7315, Centre Européen de la Céramique, 12 Rue Atlantis, 87068 Limoges, France

⁵Institut des Nanotechnologies de Lyon, INSA Lyon, Université de Lyon, UMR CNRS 5270, avenue Capelle, 69621 Villeurbanne, France

(Received 10 September 2014; accepted 5 December 2014; published online 16 December 2014)

Thin films of the lead-free ferroelectric $\text{Na}_{0.5}\text{Bi}_{0.5}\text{TiO}_3$ grown on thin-film Pt electrodes supported by SrTiO_3 substrates have a complex microstructure consisting of crystalline grains with three distinct major crystallographic orientations. The piezoelectric response measured in spatially separated sub-micron grains using time-resolved synchrotron x-ray microdiffraction is highly inhomogeneous even among grains sharing the same major orientation. The piezoelectric coefficient d_{33} varies by nearly a factor of two in a series of areas sharing the $\langle 001 \rangle$ orientation. The piezoelectric inhomogeneity is linked to the peculiar microstructure of the film, arising from local variations in the stress imposed by surrounding grains with different crystallographic orientations and differing directions of the ferroelectric remnant polarization. A systematic nonlinearity of the piezoelectric strain is observed in applied electric fields with small magnitudes in all regions, consistent with the coexistence of domains of differing polarization direction at zero applied electric field. © 2014 AIP Publishing LLC. [<http://dx.doi.org/10.1063/1.4904458>]

The development of ferroelectric materials with enhanced electromechanical response,¹ reduced toxicity,² and reduced dimensions^{3,4} is an important challenge. The functional properties of ferroelectrics, including high dielectric constants and piezoelectricity, depend on a complex interplay between local chemical and physical effects and long-range elastic and electrical boundary conditions. The strain imposed by the substrate or by the surrounding ferroelectric material and the magnitude of the depolarizing electric field each depend in turn on the microstructure and spatial extent of the ferroelectric layer and the structure and composition of its electrode interfaces.⁵ Thin films of promising lead-free ferroelectrics often exhibit structural inhomogeneity arising from the random nature of nucleation and from the generation of structural defects during growth. Laterally separated mosaic blocks, or grains, can have different crystallographic orientations, often with sub-micron lateral dimensions.⁶ Controlling and understanding the resulting inhomogeneity is the key to employing these materials, particularly in applications demanding layers with thicknesses greater than the threshold thickness for plastic relaxation during epitaxy, which is only a few tens of nm on common

substrates. For widely studied materials, such as the rhombohedral multiferroic BiFeO_3 , aspects of the structural inhomogeneity are beginning to be understood.⁷ The relationship between structural and functional properties is well-described only on an average basis,⁵ in part, due to a lack of experimental probes combining piezoelectric and structural sensitivity at the appropriate length scale. Tightly focused x-ray beams are an important local probe in this respect because x-ray scattering has high structural sensitivity to structural parameters. In this letter, we show results from thin films of the lead-free ferroelectric $\text{Na}_{0.5}\text{Bi}_{0.5}\text{TiO}_3$ (NBT). Using time-resolved x-ray microdiffraction, we show that thin NBT films have a wide distribution of piezoelectric properties arising from the local environment of individual grains, reflecting the structural inhomogeneity of the thin film. The results indicate that in this thickness regime NBT, and other similar ferroelectrics with rhombohedral or monoclinic crystal structures, exhibit a mesoscopic dependence of piezoelectric distortion on the elastic environment, an effect that is familiar from bulk piezoelectric ceramics.^{8,9}

NBT is a promising lead-free substitute for $\text{Pb}(\text{Zr,Ti})\text{O}_3$, with large ferroelectric remnant polarization ($P_r = 39 \mu\text{C}/\text{cm}^2$), low coercive electric field ($E_c = 69 \text{ kV}/\text{cm}$),¹⁰ and large piezoelectric coefficients.^{11,12} Single crystals of NBT, for example, have values of the d_{33} piezoelectric coefficient of $65 \text{ pm}/\text{V}$.¹³ The NBT crystal structure has been previously described using rhombohedral symmetry,¹⁴ or using a monoclinic space group C_c .^{15–17} Electron diffraction studies of individual domains within a multi-domain NBT sample show rhombohedral symmetry,¹⁸ and suggest that monoclinic symmetry arises from a macroscopic average.¹⁹ The

^{a)}Electronic mail: gerardina.carbone@maxlab.lu.se. Present address: MAX IV Laboratory, Ole Römers väg 1, 223 63, Lund, Sweden

^{b)}Present address: Institut FRESNEL - Av. Escadrille Normandie-Niemen 13397 Marseille, France

^{c)}Electronic mail: evans@engr.wisc.edu

^{d)}Present address: IM2NP (UMR 7334), Aix-Marseille Université, CNRS, Faculté des Sciences, Campus de Saint-Jérôme, Avenue Escadrille Normandie Niemen Case 142, F-13397 Marseille, France

^{e)}Present address: Univ. Grenoble Alpes, F-38000 Grenoble, France; CEA LETI, MINATEC Campus, 17 rue des Martyrs, F-38054 Grenoble, France

^{f)}Electronic mail: jean-rene.duclere@unilim.fr

structure is sufficiently close to cubic, however, that the structural results in this letter are presented in terms of a simplified pseudocubic structure with lattice parameter $a = 3.89 \text{ \AA}$. With this notation, the ferroelectric remnant polarization is along the $\langle 111 \rangle$ body diagonal, leading to eight different orientations for the polarization vector for each orientation of the pseudocubic unit cell. For $\langle 001 \rangle$ -oriented regions within thin films the polarization vector is thus systematically misoriented with respect to the surface normal, and a complex domain structure is likely adopted in order to minimize the total elastic and electrostatic energy.²⁰

Thin films of NBT with a thickness of 450 nm were grown by pulsed laser deposition on an epitaxial Pt (111) electrode supported by a SrTiO₃ (111) single crystal substrate.²¹ Circular Pt electrodes with diameter of 340 μm and a thickness of 300 nm were deposited on the top surface to form thin-film capacitors. The thin film growth of NBT yields grains of three different major crystallographic orientations with lateral sizes of 0.1–1 μm , as is apparent in the scanning electron microscopy (SEM) image in Fig. 1(a). The three crystallographic orientations coexisting along the surface normal are $\langle 001 \rangle$, which forms the uniform background layer in Fig. 1(a), and $\langle 110 \rangle$ and $\langle 111 \rangle$, apparent as grains with two- and three-fold symmetry, respectively. Transmission electron microscopy and laboratory x-ray diffraction studies confirm the identification of these grain orientations. Each family of grains also exhibits preferential orientation in the plane of the film.²²

The electromechanical properties of the NBT layer were investigated using x-ray microdiffraction at beamline ID01 of the European Synchrotron Research Facility in Grenoble. Monochromatic x-rays with 8.50 keV photon energy were focused by a 200 μm -diameter Au Fresnel zone plate to a spot with dimensions of 300 nm and 500 nm in the vertical and horizontal directions, respectively. Two-dimensional

scanning x-ray diffraction maps of the structure of the NBT layer were obtained by optimizing the diffraction conditions for selected Bragg reflections and rastering the sample beneath the focused beam.²³ The variation of the intensity of the diffracted beam in images formed using the (002) and the (220) Bragg reflections in two different areas, Fig. 1(b), is consistent with the discontinuous microstructure observed using SEM. Despite being an unsought feature in the fabrication of the oxide films, this discontinuous microstructure has been crucial for the study of the inhomogeneity in the lattice strain response. Electrical contact to the top electrode was made through a probe tip positioned by a remotely controlled xyz stage.²⁴ The applied voltage was connected to the bottom Pt electrode of the NBT capacitors while the top Pt electrode was connected to a virtual-ground preamplifier. The experimental arrangement was similar to previous studies of the piezoelectric response of uniform Pb(Zr,Ti)O₃ thin films using millisecond or nanosecond duration electric-field pulses.^{25,26} Here, the lateral resolution provided by the focused x-ray beam is exploited to select specific regions of the sample and probe separately their mechanical response.

The converse piezoelectric effect leads to a systematic variation of the lattice parameter of the NBT thin film in an externally applied electric field. The magnitude of the piezoelectric strain of separated grains was determined by measuring the electric-field-induced angular shift of NBT x-ray reflections. The electric field for the time-resolved diffraction study was produced using 100 repetitions of a triangular voltage pulse with a full-cycle duration of 10 ms and amplitude of 8 V. The maximum applied voltage corresponded to a nominal electric field $E = 178 \text{ kV/cm}$. The sequence of pulses was repeated several times at each angular setting of a θ - 2θ scan in order to obtain adequate counting statistics in the measurement of the intensity of the diffracted beam. The applied waveforms consisted of positive half-cycles of the

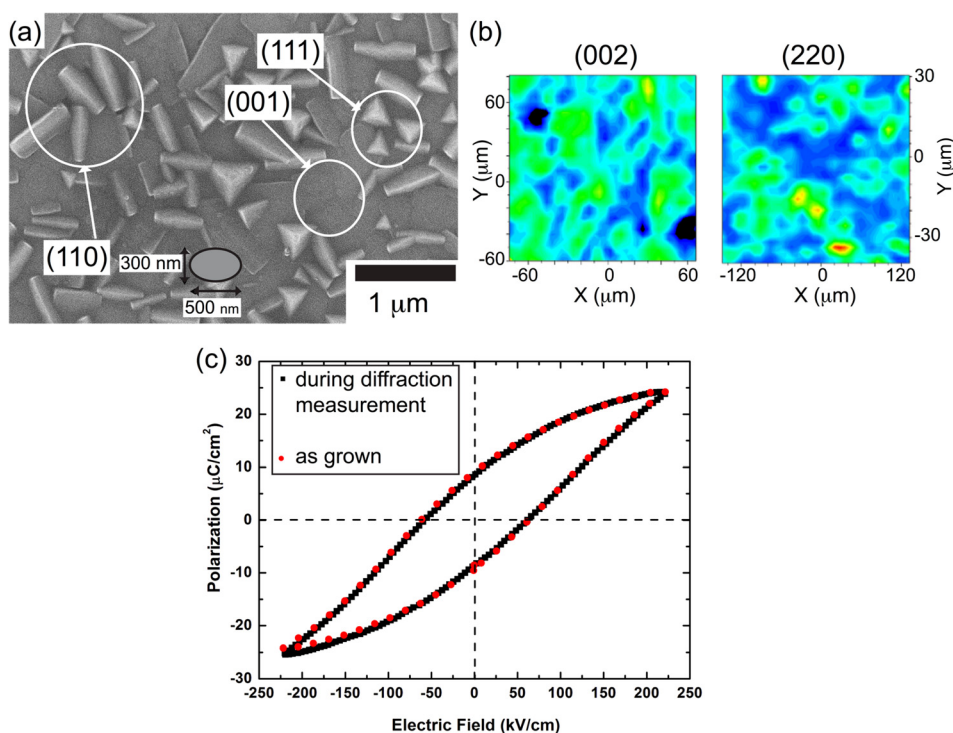


FIG. 1. (a) Scanning electron micrograph of the morphology of the NBT thin film. Grains of distinct shapes arise from the $\langle 001 \rangle$, $\langle 110 \rangle$, and $\langle 111 \rangle$ crystallographic orientations produced during deposition. Cross-sectional SEM²² measurements show that the $\langle 001 \rangle$ -oriented grains have uniform thickness. An example of the approximate extent of the scanned focused x-ray beam is indicated by the gray ellipse. (b) Scanning x-ray diffraction microscopy images in two different areas measured at the (002) and the (220) Bragg reflections. (c) Polarization-electric field hysteresis loop measured during the synchronized x-ray measurements and a hysteresis loop of the as-grown sample.

triangle wave, negative half-cycles, or a full bipolar cycle. The diffraction signal and the current were measured in time bins of 0.5 ms synchronized with the external applied electric field using a multi-channel scaler.²⁵ Electrical measurements were used to construct polarization-electric field ($P(E)$) hysteresis loops during the x-ray experiments and to monitor the leakage current, an important issue in NBT thin films.²⁷ The $P(E)$ curve acquired during the x-ray measurement in Fig. 1(c) was identical to the room temperature macroscopic ferroelectric hysteresis loop acquired following growth, indicating that the properties observed in the x-ray study are representative of as-grown layers.

The applied voltage and simultaneously recorded diffraction signal from the (002) reflection of one of the measured (001)-oriented grains are shown in Fig. 2 for measurements with a positive half-cycle electric field waveform. The wave vector of the maximum intensity, $q_{max}(t)$, is determined at different times t , and used to obtain the d-spacing of the (002) reflection as a function of time, $d^{002}(t) = 2\pi/q_{max}(t)$. The values of the wave vector of the maximum intensity are shown for representative measurements using a positive half-cycle waveform and a bipolar triangular waveform in Figs. 3(a) and 3(b), respectively. The strain induced by the applied electric field is calculated using

$$\epsilon(t) = \frac{d^{002}(t) - d_0^{002}}{d_0^{002}}. \quad (1)$$

The strain is thus defined using the difference between $d^{002}(t)$ and the reference value d_0^{002} at $E = 0$ kV/cm. The dependence on the external field is extracted via the synchronization of the applied voltage and diffraction signals. The local longitudinal piezoelectric coefficient d_{33} is obtained from the strain $\epsilon(t)$ using

$$\epsilon(E) = d_{33}E. \quad (2)$$

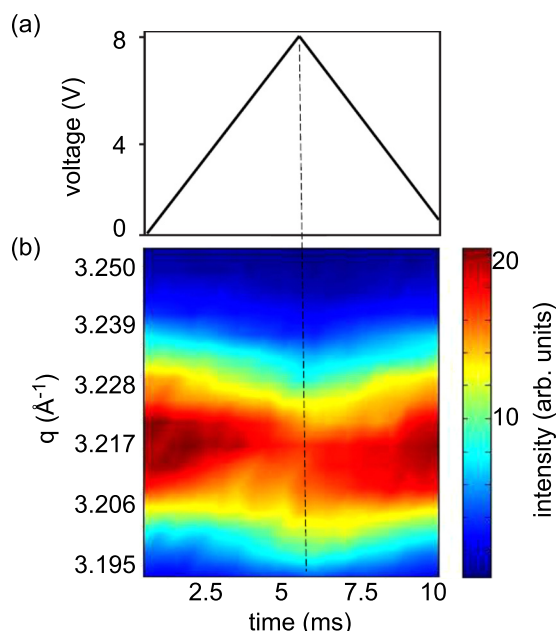


FIG. 2. (a) Positive half-cycle triangular voltage waveform for piezoelectric measurements. (b) Intensity of the NBT (002) Bragg reflection as a function of wave vector and time during the pulse shown in (a).

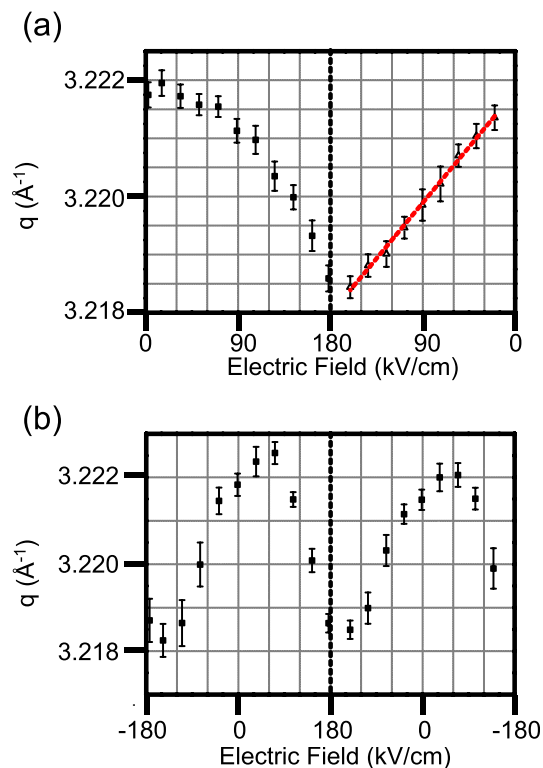


FIG. 3. (a) Magnitude of the wave vector of maximum diffracted intensity q_{max} during application of positive half-cycle triangular voltage pulses. The line is the fit to the data for decreasing field amplitudes. (b) q_{max} during application of a bipolar triangle waveform.

The shift in q_{max} and the strain $\epsilon(E)$ systematically deviate from linearity for small values of the increasing applied voltage, as shown in Fig. 3(a), while a clear linear behaviour is observed for decreasing applied voltages. An examination of the polarization-electric field hysteresis loop in Fig. 1(c) shows that polarization switching occurs over the complete range of magnitudes of the applied field. The piezoelectric nonlinearity can thus be linked to the initial switching of the polarization in some ferroelectric domains to an orientation in which the projection of the polarization onto the surface normal is parallel to the applied field. For increasing electric field (cf. Fig. 3(a)) polarization domains remain in a preferred zero-field configuration and hinder the piezoelectric expansion. Including these low-field results in the extraction of the d_{33} coefficient thus leads to an underestimation of its effective value. The domain configuration persists despite a pre-poling step lasting for 20 min at 220 kV/cm before the diffraction experiments. This diversity of polarization domains within the region illuminated by the focused x-ray beam shows up as an increase of the width of the Bragg reflections from $0.0222 \pm 0.001 \text{ \AA}^{-1}$ full-width at half maximum (fwhm) at $E = 0$ kV/cm to $0.0236 \pm 0.001 \text{ \AA}^{-1}$ fwhm at the maximum applied field. The non-linearity of the piezoelectric response is, therefore, the signature of the reversal of the polarization for a fraction of the ferroelectric domains within each grain. Domain wall motion results from such reversal. When the electric field is switched off, some of the polarization vectors flip back in a preferential orientation. This effect, known as “self-polarization,” has been already observed in $\text{Pb}(\text{Zr},\text{Ti})\text{O}_3$.^{28,29} Piezoelectric force microscopy (PFM) measurements performed on this film confirm this

behavior showing a rapid reversal of the phase of the lock-in amplifier after the removal of the electric field.³¹ The domain pattern returns to the preferred mixed-polarization state over a period of time at zero electric field following each electric field pulse. The delay between repetitions of each pulse was 0.5 ms, placing an upper limit on the time for which the poled configuration of the domains is retained. A similar relaxation due to self-polarization has been also observed by PFM studies of similar NBT layers grown on epitaxial Pt electrodes on (100) MgO single crystal substrates.³⁰

For decreasing fields, the direction of the polarization is unchanged and thus the response of the system is linear, as in Fig. 3(a). In contrast, the structural response to bipolar triangle waveforms is nonlinear throughout its entire range, as is apparent in the dependence of q_{max} on electric field during bipolar voltage pulses shown in Fig. 3(b). The nonlinearity indicates that there is incomplete switching of the polarization during each bipolar voltage cycle.

Piezoelectric coefficients are extracted from a linear fit to the decreasing segments of the voltage pulses. The results of a series of six measurements performed on separate grains are given in Table I. The uncertainty in d_{33} from the fit to the experimental data ranges from 2 to 8 pm/V. The average value of d_{33} is 65 pm/V similar to the value of 65 pm/V measured on the (001)-oriented NBT single crystals.³²

Close examination of the values in Table I shows, however, that the dispersion of the values of d_{33} around the average value is far larger than the uncertainty associated with the fit to Eq. (2). A variation of stoichiometry could be partly responsible for this large dispersion. Previous studies¹⁰ have found for example that d_{33} increases as the concentration of Na is decreased. However, for the NBT film studied here, X-ray diffraction data averaged over large surfaces show only traces of secondary phase(s) in the splitting of the (h00) Bragg peaks, with a new peak systematically located at lower 2θ angles. Based on the amplitude ratio of the Bragg peaks, we estimate that the volume fraction of these secondary phase(s) is approximately 2%. Moreover, for all the probed grains, the reported sub-micron x-ray beam measurements never revealed the presence of asymmetry or peak splitting, meaning that the secondary phase was never encountered. The d-spacings of the (002) Bragg reflection at zero field are equal for all of the measured grains within the resolution of the diffraction experiment ($d_0^{002} = 1.950 \text{ \AA}$), indicating that there is no systematic variation of the strain

TABLE I. Piezoelectric coefficients extracted from time-resolved x-ray diffraction measurements on six different (001)-oriented NBT grains, using the linear part of the measured strain as a function of electric field. The electric field waveforms used to carry out the time resolved X-ray microdiffraction experiments are indicated.

d_{33} (pm/V)	Electric field waveform
66 ± 2	Positive
55 ± 3	Positive
88 ± 6	Positive
48 ± 2	Negative
73 ± 8	Bipolar
92 ± 3	Bipolar

imposed on the (001) oriented grains. The intensity distribution near Bragg peaks at zero electric field is symmetric and Gaussian for all of the grains, which excludes chemical or strain gradients across the thickness of the film. SEM and TEM observation of the films cross-section indicate an overall film thickness variation of 20%–25%. However, the thickness of the (001) grains is more uniform, variations between different grains not exceeding 10%. This, along with the absence of porosity or electrode-film roughness that could affect the magnitude of the effective applied electric field,²² suggests that the dispersion of the observed values of d_{33} is linked to the film structural inhomogeneity rather than to thickness or electric field variations. The grains surrounding each point in the NBT thin film can have different crystallographic orientations, consequently different directions of the polarization vector, and thus different stresses induced by the piezoelectric response to the applied field. Because each NBT grain is tightly elastically coupled to its neighbors, the slightly different local environment for each point in the NBT film leads to a lateral variation in the d_{33} piezoelectric coefficient. A similar effect links the macroscopic elastic distortion to the piezoelectric expansion of the lattice in bulk piezoelectric ceramics.⁹

The further development of advanced thin film ferroelectric materials for electromechanical applications will require measurement and understanding of their structure and functional properties over the length scale set by their structural inhomogeneity. The large range of values of d_{33} in NBT indicates that the evaluation of thin-film materials based on their macroscopic average piezoelectric properties results in an incorrect interpretation of the actual behavior. Future optimization of piezoelectric thin film materials, including NBT, has the potential to lead to piezoelectric properties that are far better than the presently available macroscopic average. The lateral resolution of the present experiment was hundreds of nanometers, matching the length scale of the sample's morphological inhomogeneity. We note that, beyond the scope of the present results, an even smaller x-ray probe could allow to map this inhomogeneity at much smaller length scales, provide a clearer picture of the size-related physics of these materials and ultimately allow the investigation the grain boundaries. Such a probe would be greatly beneficial also in the study of epitaxial films. For perovskite materials, partial relaxation during heteroepitaxy can lead to strain gradients or to the formation of coherent domains (e.g., twins or alternating domains producing strong periodic modulation of crystal lattice without defects or grain boundaries).³³ The resulting strain inhomogeneity is expected to have a dramatic influence on the material physical properties, such as in the case of the enhancement of mechanical response by the flexoelectric effect.³⁴ The continuous technical development of x-rays nanobeam characterization techniques provides a structural probe with simultaneously high spatial and high strain resolution that will be capable of contributing substantially to the understanding of physical properties of inhomogeneous functional materials.

The authors wish to thank T. Schüllli, V. L. R. Jacques, and A. Cano for the careful reading of the manuscript and

for discussion of the results. The authors acknowledge the support of R. Homs and H. Djazouli during experiments at the ID01 beamline at ESRF and I. Snigireva for SEM measurements. This work was supported by institutional grants from the LabEX SigmaLim (ANR-10-LABX-0074-01). P.G.E. acknowledges support from the U.S. National Science Foundation Division of Materials Research through Grant No. DMR-1106050.

- ¹V. V. Shvartsman and D. C. Lupascu, *J. Am. Ceram. Soc.* **95**, 1 (2012).
- ²P. K. Panda, *J. Mater. Sci.* **44**, 5049 (2009).
- ³W. S. Yun, J. J. Urban, Q. Gu, and H. Park, *Nano Lett.* **2**, 447 (2002).
- ⁴W. Ma, C. Harnagea, D. Hesse, and U. Gosele, *Appl. Phys. Lett.* **83**, 3770 (2003).
- ⁵K. Lefki and G. J. M. Dormans, *J. Appl. Phys.* **76**, 1764 (1994).
- ⁶J.-R. Duclère, C. Cibert, A. Boule, V. Dorcet, P. Marchet, C. Champeaux, A. Catherinot, S. Deputier, and M. Guilloux-Viry, *Thin Solid Films* **517**, 592 (2008).
- ⁷C. Beekman, W. Siemons, T. Z. Ward, J. D. Budai, J. Z. Tischler, R. Xu, W. Liu, N. Balke, J. H. Nam, and H. M. Christen, *Appl. Phys. Lett.* **102**, 221910 (2013).
- ⁸D. A. Hall, A. Steuwer, B. Cherdhirunkorn, P. J. Withers, and T. Mori, *J. Mech. Phys. Solids* **53**, 249 (2005).
- ⁹J. L. Jones, M. Hoffman, J. E. Daniels, and A. J. Studer, *Appl. Phys. Lett.* **89**, 092901 (2006).
- ¹⁰M. Spreitzer, M. Valant, and D. Suvorov, *J. Mater. Chem.* **17**, 185 (2007).
- ¹¹Y. Hiruma, H. Nagata, and T. Takenaka, *J. Appl. Phys.* **105**, 084112 (2009).
- ¹²O. Elkechai, M. Manier, and J. P. Mercurio, *Phys. Status Solidi A* **157**, 499 (1996).
- ¹³S. M. Emel'yanov, I. P. Raevskii, V. G. Smotrakov, and F. I. Savenko, *Neorg. Mater.* **21**, 839 (1985).
- ¹⁴G. O. Jones and P. A. Thomas, *Acta Cryst. B* **58**, 168 (2002).
- ¹⁵S. Gorfman and P. A. Thomas, *J. Appl. Cryst.* **43**, 1409 (2010).
- ¹⁶E. Aksel, J. S. Forrester, J. L. Jones, P. A. Thomas, K. Page, and M. R. Suchomel, *Appl. Phys. Lett.* **98**, 152901 (2011).
- ¹⁷S. Gorfman, A. M. Glazer, Y. Noguchi, M. Miyayama, H. Luo, and P. A. Thomas, *J. Appl. Cryst.* **45**, 444 (2012).
- ¹⁸R. Beanland and P. A. Thomas, *Phys. Rev. B* **89**, 174102 (2014).
- ¹⁹I. Levin and I. M. Reaney, *Adv. Funct. Mater.* **22**, 3445 (2012).
- ²⁰S. K. Streiffer, C. B. Parker, A. E. Romanov, M. J. Lefevre, L. Zhao, J. S. Speck, W. Pompe, C. M. Foster, and G. R. Bai, *J. Appl. Phys.* **83**, 2742 (1998).
- ²¹M. Bousquet, "Croissance, caractérisations et étude des propriétés physiques de films minces du matériau ferroélectrique Na_{0.5}Bi_{0.5}TiO₃," Ph.D. thesis, University of Limoges, France, 2010.
- ²²See supplementary material at <http://dx.doi.org/10.1063/1.4904458> for details on electrical and structural characterisation.
- ²³J. Stangl, C. Mocuta, V. Chamard, and D. Carbone, *Nanobeam X-Ray Scattering: Probing Matter at the Nanoscale* (Wiley-VCH Verlag GmbH & Co. KGaA, Weinheim, Germany, 2013).
- ²⁴T. W. Cornelius, A. Davydok, V. L. R. Jacques, R. Grifone, T. Schüllli, M.-I. Richard, G. Beutier, M. Verdier, T. H. Metzger, U. Pietsch, and O. Thomas, *J. Synchrotron Radiat.* **19**, 688 (2012).
- ²⁵D.-H. Do, A. Grigoriev, D. M. Kim, C.-B. Eom, P. G. Evans, and E. M. Dufresne, *Integr. Ferroelectr.* **101**, 174 (2008).
- ²⁶A. Grigoriev, R. Sichel, H.-N. Lee, E. C. Landahl, B. Adams, E. M. Dufresne, and P. G. Evans, *Phys. Rev. Lett.* **100**, 027604 (2008).
- ²⁷M. Li, M. J. Pietrowski, R. A. De Souza, H. Zhang, I. M. Reaney, S. N. Cook, J. A. Kilner, and D. C. Sinclair, *Nat. Mater.* **13**, 31 (2014).
- ²⁸V. P. Afanasjev, A. A. Petrov, I. P. Pronin, E. A. Tarakanov, E. J. Kaptelov, and J. Graul, *J. Phys.: Condens. Matter* **13**, 8755 (2001).
- ²⁹A. Wu, P. M. Vilarinho, V. V. Shvartsman, G. Suchanek, and A. L. Kholkin, *Nanotechnology* **16**, 2587 (2005).
- ³⁰M. Bousquet, J.-R. Duclère, C. Champeaux, A. Boule, P. Marchet, A. Catherinot, A. Wu, P. M. Vilarinho, S. Deputier, M. Guilloux-Viry, A. Crunteanu, B. Gautier, D. Albertini, and C. Bachelet, *J. Appl. Phys.* **107**, 034102 (2010).
- ³¹J.-R. Duclère (private communication, 2013).
- ³²W. Ge, H. Liu, X. Zhao, W. Zhong, X. Pan, T. He, D. Lin, H. Xu, X. Jian, and H. Luo, *J. Alloys Compd.* **462**, 256 (2008).
- ³³U. Gebhardt, N. V. Kasper, A. Vigliante, P. Wochner, H. Dosch, F. S. Razavi, and H.-U. Habermeier, *Phys. Rev. Lett.* **98**, 096101 (2007); C. J. M. Daumont, D. Mannix, S. Venkatesan, G. Catalan, D. Rubi, B. J. Kooi, J. T. M. De Hosson, and B. Noheda, *J. Phys.: Condens. Matter* **21**, 182001 (2009).
- ³⁴G. Catalan, A. Lubk, A. H. G. Vlooswijk, E. Snoeck, C. Magen, A. Janssens, G. Rispens, G. Rijnders, D. H. A. Blank, and B. Noheda, *Nat. Mater.* **10**, 963 (2011).